BLIND SEPARATION OF SPATIALLY INDEPENDENT COMPONENTS FROM $H_2{}^{15}O$ DYNAMIC MYOCARDIAL POSITRON EMISSION TOMOGRAPHY

Jae Sung Lee, Ji Young Ahn, Myoung Jin Jang, Kwang Suk Park, and Dong Soo Lee

Department of Nuclear Medicine, Seoul National University College of Medicine,
28 Yungun-Dong, Chongno-Gu, Seoul 110-744, Korea
E-mail: jaes@snuvh.snu.ac.kr and dsl@plaza.snu.ac.kr

ABSTRACT

We applied the ICA method to separate the ventricle and tissue components and to extract left ventricular input function from the $H_2{}^{15}O$ myocardial PET under the assumption that the elementary activities of ventricular pools and myocardium were spatially independent, and that the mixture of them composed dynamic PET frames. ICA-generated left ventricular input functions were compared with the ROI-generated ones, and also with the invasively derived arterial blood samples. Moreover, the rMBF calculated with the ICA-generated input functions and single compartment model was correlated with the results obtained with the radiolabeled microspheres.

1. INTRODUCTION

Based on the differential equation for the kinetics of radiopharmaceutical, regional myocardial blood flow (rMBF) can be estimated using the time activity curve (TAC) of the blood pool and myocardial tissue measured by positron emission tomography (PET)[1]. In the quantification of rMBF using $H_2{}^{15}O$ dynamic PET, the input TAC could be obtained by sampling the blood from the artery or by drawing the region of interest (ROI) on the left ventricular (LV) area in the PET image. Arterial blood sampling is too uncomfortable method for both the patients and operator since it should be performed several times during the PET scanning in rapid manner. In contrast, the non-invasiveness in the method of drawing the ROI could reduce the patients and operator's burden.

It is, however, hard to identify the anatomical structure of the LV on a PET image to draw the ROI [2]. The reason is because $H_2{}^{15}O$ with bolus injection is rapidly and evenly distributed over the whole cardiac regions, such as the left and right ventricle (RV) and myocardial tissues as shown in Figure 1. It was, therefore, necessary to equip the additional device to generate radioactive-gas and to acquire $C^{15}O$ PET image for the determination of the LV area to obtain the exact LV input function [1].

Factor analysis has been proposed to extract the LV input function and tissue TAC from the $H_2{}^{15}O$ PET without $C^{15}O$ PET scanning [2]. Although the factor analysis is considered as an attractive tool to process dynamic image sequences, the problem of non-uniqueness of the solution and the additional assumptions of a *priori* knowledge to solve the problem make the user of this method cumbersome [3], [4].

Biomedical application of the blind source separation by Independent Component Analysis (ICA) has received considerable attention because of its plausibility to biomedical signals [5], [6], [7]. In this study we applied this fairly novel approach to the problem of noninvasive extraction of LV input function from the $H_2{}^{15}O$ dynamic myocardial PET image.

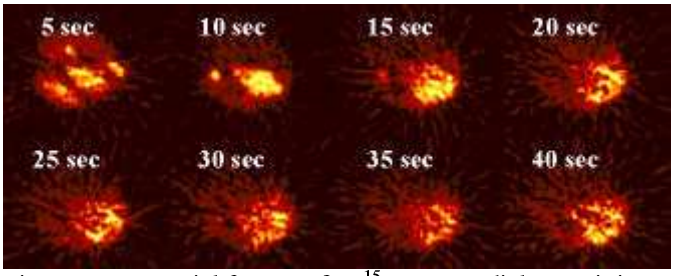

Figure 1. Sequential frames of $H_2{}^{15}O$ myocardial PET: it is difficult to define anatomical structures exactly because of the rapid distribution of $H_2{}^{15}O$ to the whole cardiac regions and low signal to noise ratio due to the short acquisition time.

2. METHOD

2.1. Image Acquisition and Reconstruction

$H_2{}^{15}O$ PET scans were performed on five dogs at rest and dipyridamole-induced stress using an ECAT EXACT 47 scanner (Siemens-CTI, Knoxville, USA), which has an intrinsic resolution of 5.2 mm FWHM (full width at half

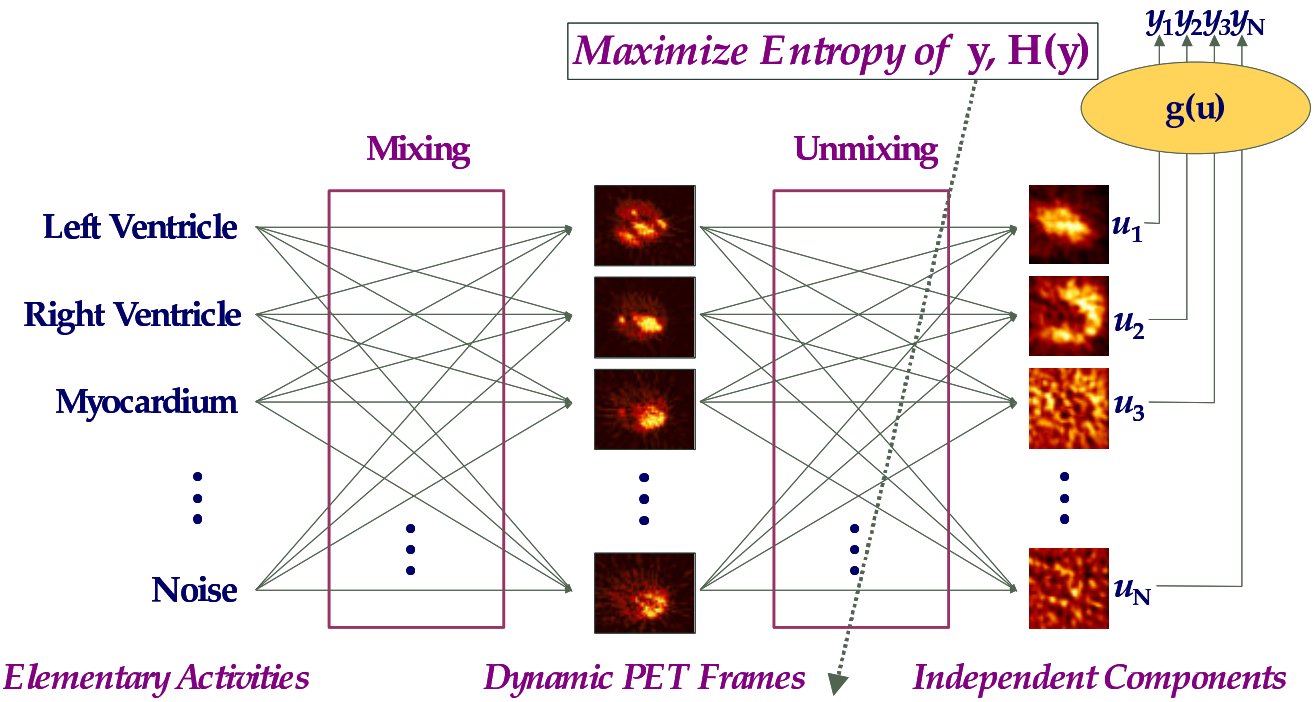

Figure 2. Schematic diagram of the processor for the blind source separation problem: demixer extracts the estimates **u**(p) of the independent source signal **s**(p) from the mixed input data **x**(p) by adjusting the weights between its input and output nodes.

maximum) and images 47 contiguous planes with thickness of 3.4 mm simultaneously for a longitudinal field of view of 16.2 cm. Before $H_2{}^{15}O$ administration, transmission scanning was performed using three Ge-68 rod sources for attenuation correction. Dynamic emission scans (5sec×2, 10sec×9, 30sec×3) were initiated simultaneously with the injection of 555~740 MBq $H_2{}^{15}O$ and continued for four minutes. Arterial blood samples were acquired at 5 seconds interval for the first 2 minutes.

Transaxial images were reconstructed by means of a filtered back-projection algorithm employing a Shepp-Logan filter with cut-off frequency of 0.3 cycles/pixel as 128×128×47 matrices with a size of 2.1×2.1×3.4 mm.

2.2. Preprocessing of $H_2{}^{15}O$ PET image

Initial eighteen frames (two minute) of PET images were used for analysis. To increase the signal to noise ratio, contiguous three reconstructed slices were summed with each other.

On the transverse slices of static images containing the biggest heart, original images were masked to reduce the extracardiac noise and include only cardiac component. Masked images with 32×32 pixels were extracted automatically. Binary images of cardiac region were composed of the pixels above 10% of global maximum pixel value of the transverse slice.

The resulting masked images with dimension of 32×32×18 (pixel×pixel×frame) were reformatted to 18×1024 (frame× pixel) matrices for further analysis.

2.3. Independent Component Analysis

We assumed that the elementary activities of ventricular pools and myocardium were spatially independent, and that the mixture of them composed dynamic myocardial PET frames as following equations.

$$\begin{aligned} X_1 &= A_{LV,1}\times S_{LV} + A_{RV,1}\times S_{RV} + A_{TI,1}\times S_{TI} \\ X_2 &= A_{LV,2}\times S_{LV} + A_{RV,2}\times S_{RV} + A_{TI,2}\times S_{TI} \\ &\vdots \\ X_N &= A_{LV,N}\times S_{LV} + A_{RV,N}\times S_{RV} + A_{TI,N}\times S_{TI} \end{aligned} \quad (1)$$

where, the random variables S_{LV}, S_{RV} and S_{TI} represent the elementary activities corresponding to the left and right ventricular pool and myocardial tissue, respectively.

Since their anatomical structures are not overlapped in the 3-dimensional space, they could be regarded as independent sources. X_i is the PET image matrix of ith frame and time dependent coefficient $A_{..,i}$ represents the contribution of the activity of each anatomical structure to the PET image of each frame. The vector [$A_{..,1}$ $A_{..,2}$ ···

A..,$_N$] corresponds to the TAC of each structure. Equation (1) could be represented in matrix formulation as follows.

$$\mathbf{X} = \mathbf{A} \cdot \mathbf{S} \tag{2}$$

where **S** is the matrix of independent component map, **A** is the mixing matrix of which each column corresponds to the TAC of each component, and **X** is the PET data matrix.

The goal of blind source separation using ICA is to find a linear transformation **W** of the mixed signal **X** in order to make its outputs as independent as possible, which is written as

$$\mathbf{U} = \mathbf{W} \cdot \mathbf{X} = \mathbf{W} \cdot \mathbf{A} \cdot \mathbf{S} \tag{3}$$

where the **U** is an estimate of the sources [8]. Schematic diagram of this process is shown in Figure 2.

Before application of ICA, principal component analysis (PCA) using singular value decomposition (SVD) was performed to decorrelate the input images. The first four components with the largest variances were selected as input data for ICA and the remaining noise components were discarded.

ICA unmixing process was performed using the extended infomax learning algorithm proposed in [10] to maximize the joint entropy provides a simple learning rule for sources with a variety of distributions. Neural network with four input and four output nodes was trained to perform the ICA process. All the data points were passed 25 times into the network through the learning rule using a block size of 100 for batch learning. The learning rate was fixed at 0.0005. Log-likelihood of the point distribution function described as following equation [10] was computed continuously to measure the independency of the output of network and determine the optimal repetition time of the training.

$$L(\mathbf{u}, \mathbf{W}) = \log|\det(\mathbf{W})| + \sum_{i=1}^{N} \log p_i(u_i) \tag{4}$$

TAC of each independent component was obtained from the each column of the mixing matrix **A** in (3), which was computed using the pseudo-inverse of the matrix of finally estimated source data, **U**. If we replace the source data matrix **S** in (3) with the estimates **U** and multiply both side with its pseudo-inverse, $\mathbf{U}^T(\mathbf{U}\cdot\mathbf{U}^T)^{-1}$, mixing matrix **A** can be obtained simply as

$$\mathbf{A} = \mathbf{X} \cdot \mathbf{U}^T (\mathbf{U} \cdot \mathbf{U}^T)^{-1} \tag{5}$$

True left ventricular input function was obtained by rescaling the independent components which corresponded to the input TAC by the similar way that Wu and her collegues used in their factor analysis for FDG and amonia PET data [11]. The TAC was rescaled so as that its maximum value have the same value as the average of the counts above a threshold (70% of the maximum) in the corresponding dynamic frame of PET image.

2.4. Myocardial Blood Flow Estimation

We computed rMBFs using the input function by the ICA and compared them with those by the ROI method. Tissue and blood pool TACs were obtained from the manually drawn ROI on the image of myocardium that was made by simple subtraction of the initial 30 seconds' image from the two minutes' one.

rMBF was estimated using single compartment model [12]. Radioactivity in myocardial tissue can be described by the following equation.

$$C_T(t) = \frac{F}{V} C_a(t) \otimes \exp(\frac{-Ft}{V\lambda}) \tag{6}$$

where ⊗ denotes the convolution integral, $C_T(t)$ is tissue TAC observed in myocardial region (counts/g), $C_a(t)$ is the arterial blood input function (counts/ml), F/V is the rMBF per unit of tissue volume (ml/g/min), and λ is tissue/blood partition coefficient (ml/g).

Since partial volume and spillover effects contaminate the TAC observed in PET image, the tissue TAC should be related to the true activities by the following relationships.

$$C_{T,PET}(t) = F_{MM}\left[\frac{F}{V} C_a(t) \otimes \exp(\frac{-Ft}{V\lambda})\right] + F_{BM} \cdot C_a(t) \tag{7}$$

where, $C_{T,PET}(t)$ is observed PET tissue activity (counts/g), F_{MM} is recovery coefficient of tissue activity, and F_{BM} is fraction of blood activity observed in tissue activity.

Total sixty tissue TACs (six per each image) were fitted to (7) to estimate F/V, F_{MM}, and F_{BM} with the fixed partition coefficient (λ=0.92). Correlation coefficient between the rMBFs by the both methods was computed.

Moreover, the rMBF calculated with the ICA-generated input functions and single compartment model was correlated with the results obtained with the radiolabeled microspheres (n=5 dogs).

3. RESULT

In all the cases, LV input functions were extracted successfully by the ICA method. The log-likelihood increased rapidly and reached plateau between 15 and 20 repetition of training as shown in Figure 3. The results were consistent in all the canine studies. Even though we

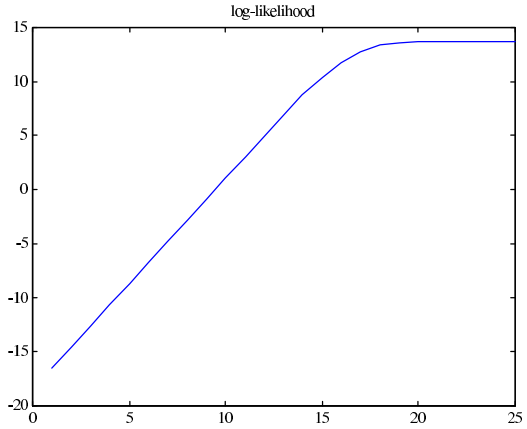

Figure 3. Plot of the log-likelihood of the PDF of the observation during the training as a function of repetition time: it increased rapidly and reached plateau between 15 and 20 repetition.

realized the ICA algorithm and reading process of PET image by the low speed computer language, Matlab (Mathworks, Natick, Mass., USA), computation time for whole process was less than 15 seconds on the workstation with 333 MHz CPU and 128 MB memory (DEC AlphaStation 600, Digital Equipment Corp., Maynard, Mass., USA).

Figure 4(a) shows an example of transverse slice of static image on which the ICA performed and the resulting independent component image of LV. LV was well identified in the central region of the mask. LV activities by the ICA and ROI methods are compared in Figure 4(b). Solid and dashed lines are ICA- and ROI-generated TACs, respectively. Their shapes were very similar except for the smoother tail of the ICA-generated one, which means the removal of the statistical noise in TAC.

Consequently, ICA-generated input functions showed good correlation with the ROI-generated ones (relative error=4.9±1.8 %), and showed similar shape with the arterial samples except for the time lags. rMBF with ICA ranged 0.6~3.9 ml/min/g, and showed good correlation with the result by microsphere (r=0.92, p<0.00001).

4. CONCLUSION

Using the blind source seperation by ICA, we could non-invasively extract the input function for the compartment modeling of myocardial perfusion from the $H_2{}^{15}O$ PET images. The rMBF using the LV activity by the ICA as the input function was correlated well with that by the ROI method. Since all the process was automatically achieved with very short computation time, it will be clinically useful for the quantification of the rMBF using $H_2{}^{15}O$ dynamic PET.

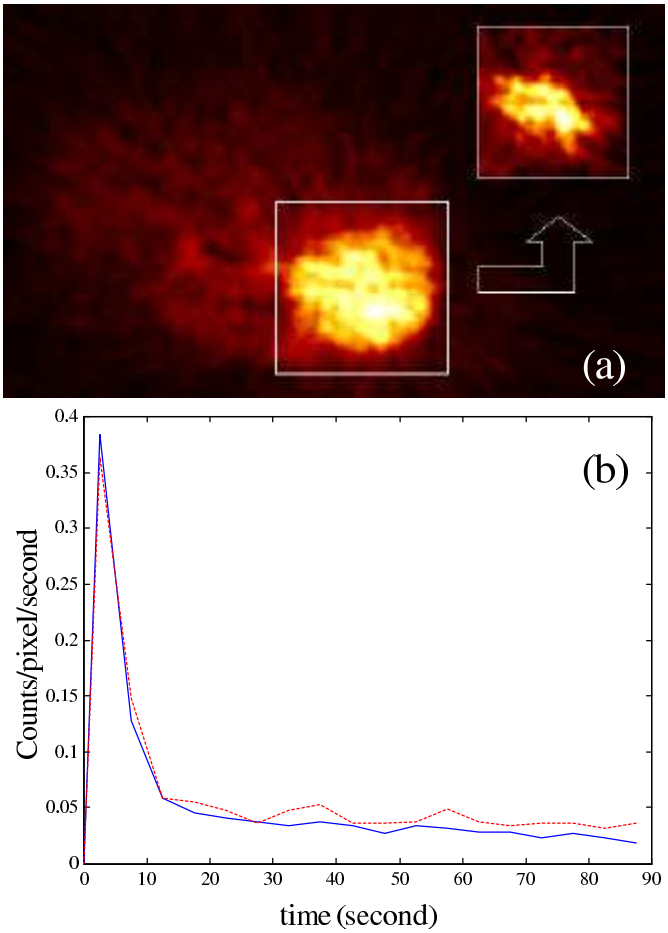

Figure 4. (a) A transverse slice of static image on which the ICA performed and the resulting independent component image of LV above the arrow: LV was well identified in the central region of the mask. (b) LV activities by the ICA and ROI methods (solid line: ICA, dashed line: ROI): their shapes were very similar except for the noiseless tail of the ICA-generated TAC.

5. REFERENCES

[1] S. R. Bergmann, K. A. A. Fox, A. L. Rand, K. D. McElvany, M. J. Welch, J. Markhan, B. E. Sobel, "Quantification of regional myocardial blood flow in vivo with $H_2{}^{15}O$", Circulation, Vol. 70, pp. 724-733, 1984.

[2] J. Y. Ahn, J. S. Lee, D. S. Lee, J. M. Jeong, J-K. Chung, M. C. Lee, "Multi-plane factor analysis for extracting input functions and tissue curves from O-15 water dynamic myocardial PET", J Nucl Med, Vol. 40(5), p. 77, 1999.

[3] A. S. Houston, "The effect of apex-finding errors on factor images obtained from factor analysis and

oblique transformation", Phys Med Biol, Vol. 29, pp. 1109-1116, 1984.

[4] A. S. Houston, W. F. D. Sampson, "A quantitative comparison of some FADS methods in renal dynamic studies using simulated and phantom data", Phys Med Biol, Vol. 42, PP. 199-217, 1997.

[5] M. J. McKeown, S. Makeig, G. G. Brown, T-P. Jung, S. S. Kindermann, A. J. Bell, T. J. Sejnowski, "Analysis of fMRI data by blind separation into independent components", Human Brain Mapping, Vol. 6, pp. 1-31, 1998.

[6] S. Makeig, M. Westerfield, T-P. Jung, J. Covington, J. Townsend, T. J. Sejnowski, E. Courchesne, "Independent components of the late positive event-related potential in a visual spatial attention task" Journal of Neuroscience, Vol. 19, pp. 2665-2680, 1999.

[7] T-W. Lee, Independent component analysis: theory and applications, Boston: Kluwer Academic Publishers., 1998.

[8] S. Haykin, Neural network: a comprehensive foundation, UK, London: Prentice-Hall, Inc., pp. 484-544, 1999.

[9] A. J. Bell, T. J. Sejnowski, "An information-maximisation approach to blind separation and blind deconvolution", Neural Computation, Vol. 7, pp. 1004-1034, 1995.

[10] T-W. Lee, M. Girolami, T.J. Sejnowski, "Independent component analysis using an extended infomax algorithm for mixed sub-gaussian and super-gaussian sources", Neural Computation, Vol. 11, pp. 417-441, 1999.

[11] H-M. Wu, C. K. Hoh, D. B. Buxton, W. G. Kuhle, H. R. Schelbert, Y. Choi, R. A. Hawkins, M. E. Phelps, S-C. Huang, "Quantification of myocardial blood flow using dynamic nitrogen-13-ammonia PET studies and factor analysis of dynamic structures", J Nucl Med, Vol. 36, pp. 2087-2093, 1995.

[12] P. Herrero, J. Markham, D. W. Myears, C. J. Weiheimer, S. R. Bergmann, "Measurement of myocardial blood flow with positron emission tomography: correction for count spillover and partial volume effects", Math Comput Model, Vol. 11, pp. 807-812, 1988.